

pubs.acs.org/Macromolecules Article

Structure—Property Relationships for Polyether-Based Electrolytes in the High-Dielectric-Constant Regime

Benjamin J. Pedretti, Natalie J. Czarnecki, Congzhi Zhu, Jennifer Imbrogno, Frederick Rivers, Benny D. Freeman,* Venkat Ganesan,* and Nathaniel A. Lynd*



Cite This: Macromolecules 2022, 55, 6730-6738



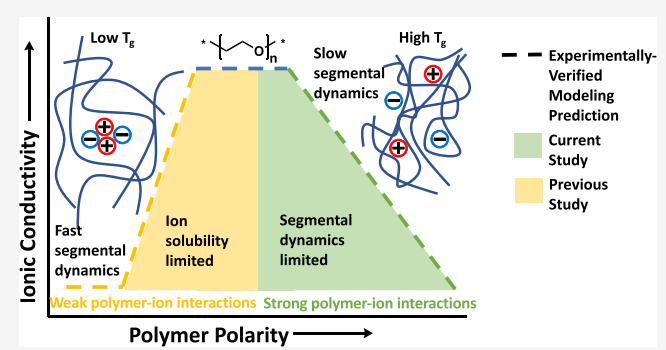
ACCESS I

III Metrics & More

Article Recommendations

s Supporting Information

ABSTRACT: Establishing general structure—property relationships for polymer electrolytes is crucial to enable design of improved materials to advance solid-state energy storage. We report the relationship between dielectric constant, glass transition temperature, and ionic conductivity for polyether-based electrolytes with dielectric constants of the polyether host within the range 7–35 at 60 °C. The ionic conductivities of the polyether and lithium bis(trifluoromethylsulfonyl)imide mixtures ranged from 10^{-7} to 10^{-3} S/cm. In this higher-dielectric-constant regime, here defined as a polymer with a dielectric constant greater than that of poly(ethylene oxide) (ca. 9.0), the glass transition temperature increased with dielectric constant while ionic conductivity



decreased. These results complement a recent report on the low-dielectric-constant regime, where the ionic conductivity was limited by the dielectric constant and ion dissociation. In the high-dielectric-constant regime explored here, segmental dynamics are slowed due to stronger polymer—polymer and polymer—ion interactions, resulting in decreased ionic conductivity and associated increase in neat polymer glass transition temperature. The disparate chemical structures of the polymers of this study, along with the results of past coarse-grained molecular dynamics simulations, support the generality of these conclusions and speak to the difficulty of identifying a single molecular characteristic leading to the design of high-conductivity polymer electrolytes. Widely used poly(ethylene oxide) represents a near-optimal balance between the low- and high-dielectric-constant regimes. To improve upon the ionic conductivity limitations of polymer electrolytes, single-component polymer hosts are unlikely to resolve the trade-off between the need for ion dissociation while retaining rapid segmental dynamics.

■ INTRODUCTION

Advances in battery technology facilitate the transition to renewable energy. To that end, polymer electrolytes can simplify battery design while increasing safety and longevity by enabling new battery chemistries.^{1,2} The disadvantage of polymer electrolytes originates from the high viscosity and slow segmental dynamics of polymers compared to those of small molecule electrolytes. This decreased ionic mobility in the polymer electrolyte host presents a significant fundamental challenge.

Current electrolytes in lithium-ion batteries contain a blend of a high-polarity, high-viscosity cyclic carbonate (e.g., ethylene carbonate) that increases ion solubility and a low-polarity linear carbonate (e.g., dimethyl carbonate) with a low viscosity that increases ion mobility. Solvents with dielectric constants (ε) below 5 will typically not fully dissolve lithium salts, leading to ionic aggregates with poor conductivities. A pure or blend polymer electrolyte may allow improvement in ionic conductivity as the dielectric constant is increased. However, previous computational work from our group predicted that increases in ionic conductivity with dielectric constant reach an

optimum as strengthening polymer—polymer and polymer—ion interactions counter increased salt dissociation. ^{6–9} Experimental validation of this hypothesis could help narrow the design parameters for a potential single polymer electrolyte or enable the redirection of research efforts away from traditional neutral polyether electrolytes based on a single polymer host.

Research into polymer electrolytes began with the discovery of ion conduction in poly(ethylene oxide) (PEO) in the 1970s. ^{10,11} PEO balances the dissociation of lithium salts while maintaining rapid segmental dynamics at high temperatures and is the most studied polymer electrolyte host. ^{12,13} PEO solvates lithium salts and exhibits conductivities over 10⁻⁴ S/cm above 70 °C. ¹⁴ Room temperature ionic conductivity of

Received: March 28, 2022 **Revised:** July 11, 2022 **Published:** July 27, 2022





PEO remains low (ca. 10^{-7} S/cm) due to semicrystallinity, which limits both the extent of amorphous material for conduction and the mobility of polymer segments. 15 While this limitation is not an issue at higher temperatures, 16 significant work remains for more relevant ambient temperature applications. Work by Barteau et al. demonstrated the applicability of glycidyl ether-based polymers, such as poly-(allyl glycidyl ether) (PAGE), in polymer electrolyte applications.¹⁴ These materials maintained higher conductivities (ca. 10⁻⁵ S/cm) than PEO at room temperature due to low glass transition temperatures and no semicrystallinity. The atactic pendant allyl groups frustrate crystallinity in both homopolymers of PAGE as well as copolymers of allyl glycidyl ether and ethylene oxide. Other work explored PEO-like materials such as (meth)acrylates with PEO side chains, 17,18 block copolymers containing PEO, ^{19–22} PEO blends with poly(ether–acetals)²³ and other analogous polymers, ²⁴ and different PEO molecular architectures. ^{25–28} Work on blends of PEO and polyacetals by Snyder et al. and Halat et al. have led to the further development of polyether materials with higher oxygen content to improve ion transport. ^{29,30} To overcome the shortcomings of polyether-based electrolytes, polymer electrolytes incorporating heteroatoms into the backbone and side chains of the polymer with functional groups such as carbonates, amines, and nitriles have also been synthesized and studied.^{31,32} Others have explored the effects of adding ionic liquid plasticizers to PEO to improve ionic conductiv--35 Segalman and co-workers have recently exploited the mechanism of superionic inorganic solid electrolytes within a polymer electrolyte material to enable selective ion motion, relying on ordered domains within polymer electrolytes to rapidly transport ions in place of the bulk polymer domain.³

Recent work has focused on understanding the mechanism of ion mobility in polymer electrolytes and structure-property relationships governing ionic conductivity. Although it is currently well recognized that low glass-transition temperature and low viscosity are important for polymer electrolyte applications, the role of polymer polarity is increasing in awareness.⁶⁻⁹ Hall et al. computationally explored how salt concentration, ion solvation, and polymer characteristics such as molecular weight influence ion transport in polymers.^{37–39} This work revealed that ion solvation governs ionic conductivity and that an increase in salt concentration can increase or decrease conductivity depending on the strength of ion-ion interactions. Kellam et al. explored how the relative population of free and associated anions in poly[bis(methoxyethoxyethoxy)phosphazene] (MEEP) affected ionic conductivity. 40 At low salt concentrations, segmental dynamics limited ion motion; however, at high salt loading, many ions existed in neutral cation-anion contact pairs and anion triplets that decreased ionic conductivity. These conclusions were also drawn from computational work by Gudla et al. that explored how ion-pair lifetimes for lithium salts in PEO affect conductivity. 41 Balsara and co-workers extensively studied salt transport mechanisms in polymer electrolytes and the factors that influence properties such as ionic conductivity.42-46

Here, we build upon on these important contributions and our previous work that explored polymers with dielectric constants lower than that of PEO (ε < 9.0) in a homologous series of poly(vinyl ether)s where conductivity was computationally predicted to be limited by salt dissociation in the polymer matrix.^{7,47} In this study, a homologous series of nine

polyether derivatives of poly(allyl glycidyl ether) containing a range of chemical functionalities on the polymer side chains that extend into the high-polarity regime with dielectric constants greater than that of PEO (ε > 9.0) were synthesized. The thermal and physical characteristics of the polymers were measured along with ionic conductivity in polymer electrolyte blends with lithium bis(trifluoromethylsulfonyl)imide (LiTF-SI). We observed a decrease in ionic conductivity of 3 orders of magnitude with a nearly 5-fold increase in dielectric constant. As predicted via molecular dynamics simulations, segmental dynamics limited ion transport as polymer—polymer and polymer—ion interactions increased with increasing dielectric constant. Maximum conductivity was achieved at moderate polarities where ion dissociation was balanced with rapid segmental dynamics.

EXPERIMENTAL SECTION

Materials. N,N-Dimethyl-2-aminoethanol (Sigma-Aldrich, \geq 99.5%), N,N-dibenzyl-2-aminoethanol (TCI, \geq 98.0%), triethylaluminum (Sigma-Aldrich, 1.0 M in hexanes), triisobutylaluminum (Sigma-Aldrich, 1.0 M in hexanes), allyl glycidyl ether (Aldrich, ≥99%), potassium osmate dihydrate (Sigma, ≥98%), N-methylmorpholine N-oxide (Acros Organics, 50 wt % solution in water), thionyl chloride (Alfa Aesar, >99%), triethylamine (Acros Organics, 99.7%), m-chloroperoxybenzoic acid (Acros Organics, 70-75% stabilized with water), 3-(allyloxy)propane-1,2-diol (TCI America, >99%), sodium hydride (Aldrich, 60% dispersion in mineral oil), methyl iodide (Acros Organics, 99%), allyl alcohol (Aldrich, ≥99%), acrylonitrile (Aldrich, ≥99%), sodium hydroxide (Sigma-Aldrich, ≥97.0%), sodium thiosulfate pentahydrate (Fisher Chemical, Certified ACS), calcium hydride (Acros Organics, ca. 93%), and sodium sulfate (Fisher Chemical, Certified ACS) were all used as received unless otherwise specified. Unless otherwise noted, all solvents were ACS reagent grade and purchased from Acros Organics, Fisher Scientific, or Sigma-Aldrich and used without further purification. CDCl₃, CD₂Cl₂, and DMSO-d₆ were purchased from Cambridge Isotope Laboratory. Lithium bis(trifluoromethane)sulfonimide (LiTFSI) salt was purchased from MilliporeSigma and stored and used in an inert nitrogen glovebox.

Polymer Characterization. 1H NMR spectroscopy was performed on a 400 MHz Agilent NMR spectrometer at room temperature and referenced to the residual solvent signal of CDCl₃ (7.26 ppm), CD_2Cl_2 (5.33 ppm), or DMSO- d_6 (2.50 ppm). Differential scanning calorimetry (DSC) was performed on a DSC250 (TA Instruments) with a RCS90 electric chiller attachment. 2.0-5.0 mg of each polymer was placed in an aluminum Tzero pan with a Tzero hermetic lid. The DSC runs were done under a nitrogen flow. The samples were heated from -90 to 40 °C at 10 °C/min, held at 40 °C for 1 min, cooled to -90 °C at 10 °C/min, and then held at -90 °C for 1 min. This was repeated two more times but to 20 °C instead of 40 $^{\circ}$ C. The third heating and cooling ramps were at 5 $^{\circ}$ C/ min. The glass transition temperature was measured by using the third heating scan. Size exclusion chromatography (SEC) was performed on an Agilent system with a 1260 Infinity isocratic pump, degasser, and thermostated column chamber held at 30 °C. An Agilent PLgel 10 μ m MIXED-B column with an operating range of 500–10000000 g/mol relative to polystyrene standards was used. This system was equipped with an Agilent 1260 refractometer and Infinity Bioinert multidetector suite featuring dual-angle static and dynamic light scattering detection. Chloroform was used as the mobile phase. FTIR was run in transmission mode on a Thermo Scientific Nicolet 6700 with a spectral resolution of 0.482 cm⁻¹. 128 scans were collected for each spectrum.

Broadband Dielectric Spectroscopy. Dielectric constant measurements were performed with a broadband dielectric spectrometer (BDS) from Novocontrol. The instrument has a high-resolution dielectric Alpha analyzer (frequency range 10^{-5} – 10^{7} Hz) and can achieve a temperature range from -160 to $400\,^{\circ}\text{C}$ via liquid

nitrogen and activated heaters. The temperatures within the cell and the Alpha analyzer are controlled by WinDETA software. A parallel-plate oriented sample cell for viscous samples was used for the dielectric measurements. The viscous polymer samples were loaded on a gold-plated lower electrode with a diameter of 40 mm with a smaller gold-plated electrode with a diameter of 20 mm placed on top. Teflon spacers of known surface area and thickness were placed between the electrodes used to control the thickness of the polymer sample. The measurement cell was kept closed by tightening the cell closing plate with spring force. Samples were measured from 10^{-2} to 10^{7} Hz and in a temperature range of $0-60\,^{\circ}$ C. The dielectric constant values were gathered by taking the average value of the plateau region of the measured real permittivity as a function of frequency. The plateau would occur typically at frequencies of $10^{1}-10^{5}$ Hz.

General Procedure for Polymer/Salt Blends Preparation. The polymers were brought into a dry nitrogen glovebox and dried *in vacuo* at room temperature for 1 day. Room temperature was above the glass transition temperature of all samples. Approximately 0.2 g of polymer was added to a tared scintillation vial with a stir bar. The vial containing polymer was then dried again *in vacuo* overnight and reweighed. The dry weight was used to calculate the amount of LiTFSI needed to be at 25 wt % salt. After the corresponding amount of LiTFSI was weighed and added to the vial, ca. 0.2 mL of THF was added to the vial, which was then allowed to stir at room temperature for 48 h. The sample was then dried *in vacuo* at room temperature until it reached the weight before solvent was added.

Electrochemical Impedance Spectroscopy. All data were collected on a BioLogic MTZ-35 impedance analyzer with an intermediate temperature system utilizing a through-plane conductivity cell. The electrode plates as well as the sample chamber were brought into the glovebox with a Teflon washer with the same diameter as the electrode. The Teflon washer served to contain the polymer electrolyte and fix the distance between the electrodes. The washer was placed on one electrode, dry polymer electrolyte was added to fill the washer, and the other electrode was placed on top and screwed in place. The electrode assembly was placed into the sample holder and sealed before being brought out of the glovebox. The EIS probes and temperature probe were then inserted into the sample holder. The sample chamber was finally placed into an insulated temperature stage. Each experiment was run in a frequency range that encompassed the full data set at all temperatures. The sample was equilibrated for an hour at each temperature before data collection on heating and cooling. The washer inner diameter (0.75 mm) and thickness (0.48 mm) were used for the sample dimensions when calculating ionic conductivity.

Synthesis of 3-(2,3-Dimethoxypropoxy)prop-1-ene. To a stirred solution of 3-(allyloxy)propane-1,2-diol (5.00 g, 1.0 equiv, 37.8 mmol) in dry THF (150 mL) chilled to 0 °C was added 3.34 g of 60% NaH stabilized in mineral oil (2.2 equiv, 83.3 mmol). The solution was allowed to stir for 30 min, at which point all gas evolution had ceased. Next, 9.42 mL of methyl iodide (4.0 equiv, 151.3 mmol) and 613.2 mg of tetrabutylammonium bromide (0.05 equiv, 1.9 mmol) were added to the reaction flask, which was allowed to warm to room temperature overnight. The next day, the reaction was quenched with 100 mL of water and extracted with diethyl ether (3 \times 100 mL). The organic layer was dried over Na2SO4, filtered, and concentrated in vacuo. The crude product was then purified by using silica gel chromatography (isocratic elution of 9:1 hexanes/EtOAc) to give the product (5.03 g, 83% isolated yield) as a clear oil. ¹H NMR (400 MHz, CDCl₃) δ : 5.97–5.84 (m, 1H), 5.33–5.12 (m, 2H), 4.01 (dt, J = 5.6, 1.5 Hz, 2H), 3.58-3.45 (m, 5H), 3.47 (s, 3H), 3.38 (s, 3H). ¹³C NMR (400 MHz, CDCl₃) δ : 134.82, 117.20, 79.41, 72.53, 69.72, 59.41, 58.09.

Synthesis of 2-((2,3-Dimethoxypropoxy)methyl)oxirane. To a stirred solution of 3-(2,3-dimethoxypropoxy)prop-1-ene (6.02 g, 1.0 equiv, 37.6 mmol) in 120 mL of dichloromethane at 0 $^{\circ}$ C was added 11.09 g of m-chloroperoxybenzoic acid (mCPBA) (1.2 equiv, 45.0 mmol) slowly. The reaction was then allowed to warm to room temperature and stirred overnight. After all of the starting alkene had

been consumed, as determined by 1 H NMR spectroscopy, the reaction was filtered to remove insoluble m-chlorobenzoic acid. The crude product was then purified by using silica gel chromatography (isocratic elution of 7:3 hexanes/EtOAc) to give the product as a clear oil. 1 H NMR (400 MHz, CDCl $_{3}$) δ : 3.73 (dddt, J = 11.6, 2.9, 2.0, 0.4 Hz, 1H), 3.63–3.34 (m, 6H), 3.42 (dd, J = 1.9, 0.6 Hz, 3H), 3.32 (dd, J = 1.1, 0.6 Hz, 3H), 3.13–3.07 (m, 1H), 2.75 (ddd, J = 4.9, 4.1, 0.6 Hz, 1H), 2.56 (dtd, J = 5.2, 2.7, 0.5 Hz, 1H). 13 C NMR (400 MHz, CDCl $_{3}$) δ : 79.30, 72.25, 72.23, 71.06, 70.97, 59.35, 58.03, 50.87, 50.84, 44.27, 44.24. m/z HRMS calculated for [M + Na] $^{+}$: 199.09; found: 199.09.

Synthesis of CEGE (2-Cyanoethyl Glycidyl Ether). 3-(Allyloxy)propanenitrile was prepared according to a reported procedure. 48 m-Chloroperoxybenzoic acid (mCPBA, 50.0 g, 0.290 mol) was dissolved in CH₂Cl₂ (600 mL) at room temperature. 3-(Allyloxy)propanenitrile (24.0 g, 0.216 mol) was added dropwise to the solution of mCPBA through an addition funnel. The mixture was stirred at room temperature for 2 days. The reaction mixture was then filtered, and the filtrate was washed with a saturated aqueous Na₂S₂O₃ solution. The organic solution was then separated and washed with a mixture of a saturated NaHCO3 solution and a NaOH (5 wt % in water) solution (v/v = 1:1) three times and with brine once. Excess CH₂Cl₂ and unreacted 3-(allyloxy)propanenitrile were removed by rotary evaporation. The crude product was further purified by distillation with from CaH2 under vacuum reduced pressure to yield the product (13.3 g, 0.104 mol, 48%), and stored in a N₂-filled glovebox. ¹H NMR (500 MHz, CDCl₃) δ : 3.88 (dd, J = 11.8, 2.6 Hz, 1H), 3.74 (ddt, *J* = 31.9, 9.5, 6.3 Hz, 2H), 3.41 (dd, *J* = 11.8, 6.0 Hz, 1H), 3.20-3.14 (m, 1H), 2.84-2.79 (m, 1H), 2.66-2.60 (m, 3H). ¹³C NMR (400 MHz, CDCl₃) δ : 117.77, 71.71, 65.82, 50.50, 43.81, 18.78. m/z HRMS calculated for $[M + Na]^+$: 150.05; found: 150.05.

General Procedure for Synthesis of Polymers. All polymerizations were performed under an inert atmosphere in a glovebox as reported previously. 49,50 In general, a scintillation vial was first charged with a stir bar and the appropriate monomer. Dimethylaminoethoxymono(μ -alkoxo)bis(isobutylaluminum) or dibenylaminoethoxymono(μ -alkoxo)bis(isobutylaluminum) was then added to the vial in the correct ratio with the monomer to target a polymer with a molecular weight of 10000 g/mol. The vial was then capped and allowed to stir at 60 °C for 2 days or until conversion plateaued as measured by ¹H NMR spectroscopy. After this, the reactions were removed from the glovebox, diluted with dichloromethane, and washed twice with a mixture of 0.1 M HCl in methanol and water (v/v = 1:9) followed by one wash with distilled water. The dichloromethane was then removed via rotary evaporation, and the sample was allowed to dry on a Schlenk line overnight. The cleaned polymers were then characterized by ¹H NMR spectroscopy and SEC.

Poly(allyl glycidyl ether) (PAGE). ¹H NMR (400 MHz, CD₂Cl₂) δ : 7.67–7.18 (m, 10H), 5.90 (ddt, J = 17.3, 10.6, 5.4 Hz, 76H), 5.26 (dq, J = 17.3, 1.7 Hz, 89H), 5.15 (dq, J = 10.4, 1.6 Hz, 86H), 3.97 (dt, J = 5.5, 1.6 Hz, 214H), 3.67–3.41 (m, 550H).

Poly(cyano ethyl glycidyl ether) (PCEGE). ¹H NMR (400 MHz, CD₂Cl₂) δ : 7.76–7.11 (m, 10H), 3.98–3.39 (m, 542H), 2.62 (t, J = 6.0 Hz, 157H).

Poly(2-((2,3-Dimethoxypropoxy)methyl)oxirane) (*PdMGE*). 1 H NMR (400 MHz, CDCl₃) δ: 4.01–3.39 (m, 200H), 3.44 (s, 60H), 3.35 (s, 60H), 1.77 (broad s, 6H).

General Procedure for the Complete and Partial Epoxidization Poly(allyl glycidyl ether). For fully epoxidized PAGE, poly(glycidyl glycidyl ether) (PGGE), 8.43 g of 75% mCPBA stabilized with water (39.3 mmol, 1.3 equiv) was added to a stirred solution of PAGE (3.01 g, 26.4 mmol of AGE repeat units, 1.0 equiv) in DCM (30 mL) over the course of 10 min. The reaction was allowed to stir for 48 h. Once the epoxidation reaction had reached 100% conversion, as confirmed by 1 H NMR spectroscopy, the reaction mixture was filtered and washed with a saturated solution of sodium bicarbonate (4 × 100 mL). The combined organic phases were then dried over Na₂SO₄, filtered, rotary evaporated, and dried in vacuo overnight. For each partially epoxidized PAGE sample (33, 66, and 85%), the corresponding percentage of mCPBA was added to the

reaction mixture with all other procedural steps identical. For 100% PGGE, 1 H NMR (400 MHz, CDCl₃) δ : 3.81–3.74 (m, 1H), 3.69–3.54 (m, 5H), 3.42–3.34 (m, 1H), 3.14 (s, 1H), 2.83–2.73 (m, 1H), 2.63–2.56 (m, 1H).

General Procedure for Upjohn Dihydroxylation of Poly(allyl glycidyl ether). Upjohn dihydroxylation was employed to partially functionalize PAGE for further synthesis of copolymers using previously reported procedures.⁵¹ For the conversion of 50% of the allyl groups to the corresponding vicinal diol, the following procedure was used. 2.02 g of PAGE was first dissolved in a mixture of 80 mL of acetone and 20 mL of water. 2.05 mL of 50 wt % N-methylmorpholine N-oxide in water (0.5 equiv) and 130 mg of K₂OsO₄ (0.02 equiv) were then added to the reaction mixture. The reaction was stirred for 2 h, after which it was quenched with the addition of 2.0 mL of saturated Na₂SO₃. The reaction was then rotary evaporated to remove the acetone, diluted with an additional 20 mL of water, and extracted with diethyl ether (3 \times 25 mL). The aqueous phase was then dialyzed against DI water for 3 days and lyophilized. Conversion of the allyl groups, as determined by ¹H NMR spectroscopy, was 53%. ¹H NMR (400 MHz, DMSO- d_6) δ : 5.87 (ddt, J = 16.5, 10.4, 5.2 Hz, 1H), 5.19 (dd, J = 45.5, 13.9 Hz, 2H), 4.56 (s, 1H), 4.44 (s, 1H), 4.01-3.88 (m, 1H)2H), 3.64-3.22 (m, 15H).

General Procedure for the Synthesis of Poly(allyl glycidyl ether-co-propylene sulfite glycidyl ether). The reaction of partially hydroxylated PAGE with thionyl chloride was employed to synthesize poly[(allyl glycidyl ether)-co-(propylene sulfite glycidyl ether)] as reported previously. 52 Briefly, 920 mg of 53% hydroxylated PAGE (0.102 mmol of polymer, 1.0 equiv) was dissolved in 75 mL of dry THF and cooled to 0 °C. 1.23 mL of triethylamine (8.8 mmol, 86 equiv) was then added, after which $SOCl_2$ (620 μL , 8.5 mmol, 84 equiv) in 10 mL of dichloromethane was added slowly to the reaction, which was then allowed to stir for 1 h. The reaction flask was then allowed to warm to room temperature for 30 min, at which point 100 mL of water was added to the reaction slowly to quench any remaining SOCl₂. The reaction was then extracted with chloroform (3 × 50 mL), after which the combined organic layers were dried over Na₂SO₄, filtered, and dried in vacuo. Complete conversion of the dihydroxyl starting material to the corresponding cyclic sulfite was confirmed with ¹H NMR spectroscopy and IR spectroscopy. ¹H NMR (400 MHz, CDCl₃) δ : 5.86 (ddt, J = 16.3, 10.8, 5.5 Hz, 1H), 5.19 (dd, J = 38.7, 13.9 Hz, 2H), 5.04 and 4.28 (each s, 1H), 4.76-4.58 (broad m, 1H), 4.52 (q, J = 8.7 Hz, 1H), 3.96 (d, J = 5.5 Hz, 2H), 3.87-3.33

RESULTS AND DISCUSSION

A homologous series of polyether derivatives of poly(allyl glycidyl ether) (PAGE) were synthesized by using a mono(ualkoxo)bis(alkylaluminum) initiator/catalyst system as reported previously. 49,50 Nine polymers and copolymers with constitutional repeat units shown in Scheme 1 were synthesized with a target molecular weight of 10000 g/mol. Polymer characteristics are shown in Table 1. The polyether series spans a range of polarity and oxygen content, which was enabled by functional group identity and incorporation onto a unified polyether backbone. The material compositions were chosen to vary the bulk physical properties such as dielectric constant and the glass transition temperature (T_{σ}) . All polymers were synthesized in 1-3 steps from commercially available precursors. The poly(dimethoxy glycidyl ether) (PdMGE) and poly(cyanoethyl glycidyl ether) (PCEGE) were polymerized from their respective monomers. Poly-(glycidyl glycidyl ether) (PGGE) and the copolymers of PAGE with PGGE and poly(sulfite glycidyl ether) (PSGE) were synthesized via postpolymerization modification of PAGE as detailed in the Experimental Section.

The materials were characterized by using nuclear magnetic resonance (NMR) spectroscopy, size exclusion chromatog-

Scheme 1. (a) Synthesis of Polyethers Using Dibenzylaminoethoxymono- μ -oxobis(triisobutylaluminum) Catalyst Initiator; (b) Postpolymerization Modification of PAGE to Form a Variety of Polar Repeat Unit Structures

(a) MOB-initiated polymerization of glycidyl ethers

(b) Derivatives synthesized for this study

PAGE PdMGE PCEGE

Tg =
$$-76.8 \,^{\circ}\text{C}$$

PGGE PSGE

-30.7 $^{\circ}\text{C}$

O

N

O

N

O

N

O

N

O

N

O

N

O

N

O

N

O

N

O

N

O

N

O

N

O

N

O

N

O

N

O

N

O

N

O

N

O

N

O

N

O

N

O

N

O

N

O

N

O

N

O

N

O

N

O

N

O

N

O

N

O

N

O

N

O

N

O

N

O

N

O

N

O

N

O

N

O

N

O

N

O

N

O

N

O

N

O

N

O

N

O

N

O

N

O

N

O

N

O

N

O

N

O

N

O

N

O

N

O

N

O

N

O

N

O

N

O

N

O

N

O

N

O

N

O

N

O

N

O

N

O

N

O

N

O

N

O

N

O

N

O

N

O

N

O

N

O

N

O

N

O

N

O

N

O

N

O

N

O

N

O

N

O

N

O

N

O

N

O

N

O

N

O

N

O

N

O

N

O

N

O

N

O

N

O

N

O

N

O

N

O

N

O

N

O

N

O

N

O

N

O

N

O

N

O

N

O

N

O

N

O

N

O

N

O

N

O

N

O

N

O

N

O

N

O

N

O

N

O

N

O

N

O

N

O

N

O

N

O

N

O

N

O

N

O

N

O

N

O

N

O

N

O

N

O

N

O

N

O

N

O

N

O

N

O

N

O

N

O

N

O

N

O

N

O

N

O

N

O

N

O

N

O

N

O

N

O

N

O

N

O

N

O

N

O

N

O

N

O

N

O

N

O

N

O

N

O

N

O

N

O

N

O

N

O

N

O

N

O

N

O

N

O

N

O

N

O

N

O

N

O

N

O

N

O

N

O

N

O

N

O

N

O

N

O

N

O

N

O

N

O

N

O

N

O

N

O

N

O

N

O

N

O

N

O

N

O

N

O

N

O

N

O

N

O

N

O

N

O

N

O

N

O

N

O

N

O

N

O

N

O

N

O

N

O

N

O

N

O

N

O

N

O

N

O

N

O

N

O

N

O

N

O

N

O

N

O

N

O

N

O

N

O

N

O

N

O

N

O

N

O

N

O

N

O

N

O

N

O

N

O

N

O

N

O

N

O

N

O

N

O

N

O

N

O

N

O

N

O

N

O

N

O

N

O

N

O

N

O

N

O

N

O

N

O

N

O

N

O

N

O

N

O

N

O

N

O

N

O

N

O

N

O

N

O

N

O

N

O

N

O

N

O

N

O

N

O

N

O

N

O

N

O

N

O

N

O

N

O

N

O

N

O

N

O

N

O

N

O

N

O

N

O

N

O

N

O

N

O

N

O

N

O

N

O

N

O

N

O

N

O

N

O

N

O

N

O

N

O

N

O

N

O

N

O

N

O

N

O

N

O

N

O

N

O

N

O

N

O

N

O

N

O

N

O

N

O

N

O

N

O

N

O

N

O

N

O

N

O

N

O

N

O

N

O

N

O

N

O

N

O

N

O

N

O

N

O

N

O

N

O

N

O

N

O

N

O

N

O

N

O

N

O

N

O

N

O

N

O

N

O

N

O

N

O

N

O

N

O

N

O

N

O

N

O

N

O

N

raphy (SEC), broadband dielectric spectroscopy (BDS), differential scanning calorimetry (DSC), and electrochemical impedance spectroscopy (EIS). A representative SEC trace and ¹H NMR spectrum are shown in Figure 1 for poly(cyanoethyl glycidyl ether) (PCEGE). For polymers synthesized via postpolymerization modification of PAGE, the starting degree of polymerization of the PAGE precursor and the degree of functionalization and formula weights of each compositional repeat unit are used to calculate the molecular weight of the final polymer. The glass transition temperatures (T_g) of the pure polymers and mixtures with 25 wt % LiTFSI are shown in Table 1. PAGE had the lowest T_g at -76.8 °C, and PGGE had the highest T_{σ} at -30.7 °C. We chose 25 wt % LiTFSI as the salt loading throughout this study because it was previously shown to be the near-optimum salt loading for PAGE. 14 Because of the variation in the different functional groups in this study and the incorporation of different heteroatoms in some of the polymers, using metrics such as molar oxygen:lithium ratios would require significantly different amounts of LiTFSI in each sample. A single salt loading was chosen as the basis for comparison.

The dielectric constant (ε) is related to the thermal fluctuations of polarization in a polar liquid. We take the dielectric constant as a measure of the *polarity* of the electrolyte polymer host without salt. The Kirkwood model relates the molecular characteristics of a polar liquid to the characteristics of the intrinsic dipoles. N is the number of dipoles in volume Ω . The orientational correlations are

Table 1. Polymer Characterization Data

polymer	$M_{\rm n}^{\ a} \ ({\rm kg/mol})$	T_{g} (°C)	$T_{g} (^{\circ}C)^{b}$	$oldsymbol{arepsilon}^c$	ionic conductivity (mS/cm) ^d
PAGE	8.8	-76.78 ± 0.13	-54.70 ± 0.10	7.48 ± 0.11	0.182
PdMGE	4.0	-69.19 ± 0.08	-49.54 ± 0.06	10.78 ± 0.16	0.114
$P(GGE_{0.33}\text{-}co\text{-}AGE_{0.67})$	9.2	-63.31 ± 0.14	-45.48 ± 1.43	10.91 ± 0.05	0.0994
$P(GGE_{0.66}$ -co- $AGE_{0.34})$	9.6	-48.61 ± 0.68	-31.36 ± 1.01	11.44 ± 0.03	0.0747
$P(GGE_{0.85}\text{-}co\text{-}AGE_{0.15})$	9.9	-47.03 ± 0.45	-36.57 ± 1.05	14.51 ± 0.38	0.0234
PGGE	10.0	-30.73 ± 1.58	-17.00 ± 2.18	16.22 ± 0.34	0.0128
$P(SGE_{0.39}\text{-}co\text{-}AGE_{0.61})$	11.2	-45.22 ± 0.36	-40.70 ± 1.32	20.24 ± 0.05	0.0535
$P(SGE_{0.53}\text{-}co\text{-}AGE_{0.47})$	12.1	-42.08 ± 0.51	-25.10 ± 0.69	22.63 ± 1.11	0.0427
PCEGE	11.0	-37.69 ± 0.24	-24.79 ± 0.59	34.51 ± 1.23	0.0363

"Number-average molecular weight determined by end-group analysis using ¹H NMR spectroscopy for homopolymers and percent conversion of functional groups from precursor polymers for copolymers. ⁵Glass transition temperature measured with 25 wt % LiTFSI. ^cDielectric constant of the pure polymer measured by broadband dielectric spectroscopy taken as the average of the plateau region of the real permittivity as a function of frequency at 60 °C. ^dIonic conductivity measured by EIS at 60 °C with 25 wt % LiTFSI.

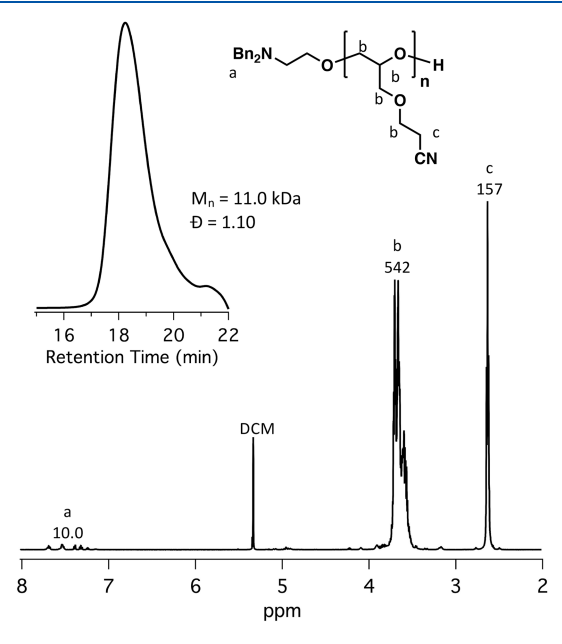


Figure 1. Representative 1 H NMR spectrum and size exclusion chromatograph (inset) for polyethers synthesized for this study. Shown is PCEGE with $M_{\rm n}=11.0$ kg/mol and D=1.10 measured by multiangle light scattering (dn/dc=0.0477 mL/g). The integrations of each resonance peak are shown on top of the corresponding peak.

captured in the Kirkwood *g*-factor (g_K) , μ is the dipole moment of a molecule in the liquid, and β is $1/k_BT$.⁵³

$$\frac{4\pi\beta N\mu^2 g_{\rm K}}{\Omega} = \frac{(\varepsilon - 1)(2\varepsilon + 1)}{\varepsilon} \tag{1}$$

Equation 1 was derived by Kirkwood using Onsager's local field approach and can be used to express ε in a short-range orientational correlation function. S4,S5 Equation 1 can be solved for the dielectric constant ε . Of the two solutions, one represents the physically meaningful expression (2) which can be used to fit and interpret the dielectric constant data.

$$\varepsilon = \frac{4\pi N \mu^{2} g_{K}^{2} + k_{B} T \Omega + \sqrt{8k_{B}^{2} T^{2} \Omega^{2} + (4\pi N \mu^{2} g_{K}^{2} + k_{B} T \Omega)^{2}}}{4k_{B} T \Omega}$$
(2)

In previous simulation results by Wheatle et al., two regimes of behavior were elucidated for polymer electrolytes with varying polarity polymer hosts.⁷ In the low-dielectric-constant

regime, ionic conductivity was limited by dielectric constant and salt dissociation and had no relationship to glass transition temperature or segmental dynamics. At higher polarity (i.e., higher dielectric constant), the ionic conductivity decreased as the dielectric constant increased. Stronger polymer-polymer and ion-polymer interactions led to higher glass transition temperatures and slower segmental dynamics. An optimum was encountered at intermediate polarity where ion dissociation was balanced against rapid segmental dynamics. All materials in this study explore the high-dielectric-constant regime. The low-dielectric-constant regime considered previously used a homologous series of poly(vinyl ether)s.⁴⁷ The hypothesis that dielectric constant and segmental dynamics limit ionic conductivity would be supported if ionic conductivity decreased with increasing polymer glass transition temperature and/or dielectric constant, and it would further be supported by correlation between dielectric constant and T_{g} both with and without salt. All of the polymers studied here had relatively low glass transition temperatures (<-30 °C) and were viscous liquids at ambient conditions.

The dielectric constants (ε) of the neat polyethers were measured by broadband dielectric spectroscopy. The dielectric constants were determined by calculating the average of the plateau region $(10^{-2}-10^7 \text{ Hz})$ of the real permittivity. Figure 2 shows the dielectric constants as a function of temperature for each polyether. As expected, PAGE had the lowest dielectric constant of ca. 7.0 at 60 °C. For the series of partially to fully epoxidized PAGE polymers (P(GGE-co-AGE)), the dielectric constant increased with increasing level of PGGE incorporation. Interestingly, the PdMGE, which has a higher oxygen content than any of the P(GGE-co-AGE) polymers, had a lower dielectric constant than $P(GGE_{0.85}\text{-}co\text{-}AGE_{0.15})$ and PGGE. The ether dipole moments may partially cancel one another in the PdMGE material, resulting in a lower dielectric constant. The polymers containing cyclic sulfite esters had higher dielectric constants than the epoxide- and ethercontaining polymers. Finally, PCEGE, with a significantly more polar side chain than the other samples exhibited the highest dielectric constant of ca. 35 at 60 °C. The data points for each polymer show good agreement with the Kirkwood

Polymer electrolytes were prepared under a dry, inert nitrogen atmosphere. LiTFSI was added to a few hundred milligrams of the polymers at a loading of 25 wt % salt (in neat polymer). The samples were mixed with ca. 0.2 mL of dry THF at room temperature for 2 days, at which point they

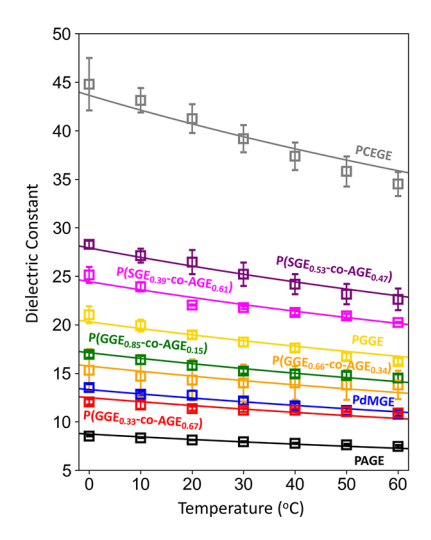


Figure 2. Dielectric constant measured for the series of polymers from 0 to 60 °C in increments of 10 °C and a frequency range of $10^{-2}-10^{7}$ Hz at each temperature. Data points were fitted with the Kirkwood model to guide the eye (eqs 1 and 2). Nonvisible error bars are smaller than data points.

appeared homogeneous. The samples were then dried in vacuo until the THF had been removed as measured gravimetrically. A single, well-defined $T_{\rm g}$ was observed for each sample both with and without salt, further indicating good polymer/salt miscibility, and in each case the $T_{\rm g}$ of the polyether with added LiTFSI was higher than that of the neat polymer.

The ionic conductivities of the polyether/salt mixtures were measured by using electrochemical impedance spectroscopy (EIS). The sealed, temperature-controlled sample stage was loaded with polymer/salt mixtures under an inert nitrogen atmosphere. The samples were allowed to thermally equilibrate for 1 h prior to each measurement at each temperature. Figure 3 shows the ionic conductivity (σ) of each sample as a function of temperature at 30–90 °C. The conductivities are plotted according to the Arrhenius format of σ vs 1000/T (K) and fit to the Vogel–Tamman–Fulcher (VTF) equation. The

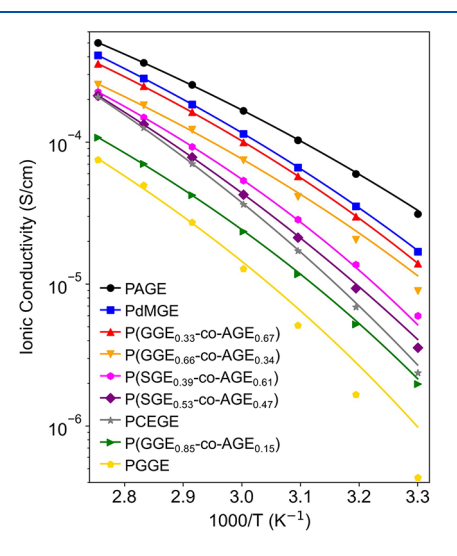


Figure 3. Conductivity data collected from 30–90 °C for each polymer with 25 wt % LiTFSI and fitted with the VTF equation. The ionic conductivities varied over nearly 3 orders of magnitude for the range of polymers over the temperatures measured.

measured conductivities span nearly 3 orders of magnitude from ca. 10^{-6} to 10^{-3} S/cm.

Previous computational and experimental work provide a framework to understand how ionic conductivity relates to correlations between the dielectric constant and glass transition temperature and how these two dynamic properties $(\varepsilon, T_{\sigma})$ are interrelated and affect ionic conductivity in different parametric regimes. 6-9,47 The comparative experimental data for the series of nine polyethers are shown in Figure 4. On the basis of the molecular dynamics simulation studies by Wheatle et al., in the range of dielectric constants the present polymer series encompasses, we expected that the ionic conductivity would no longer be limited by ion dissociation. Consequently, ionic conductivity was expected to decrease with increasing dielectric constant as polymer-polymer and polymer-ion interactions slow the rate of segmental dynamics.9 The prior computational and experimental work demonstrated that ionic conductivity increased with increasing dielectric constant in the low-dielectric-constant regime until an optimum at a dielectric constant of ca. 9.0. Further increases in dielectric constant were predicted by simulation to decrease ionic conductivity.

There was a weak and generally decreasing trend in ionic conductivity vs polymer dielectric constant in the higherpolarity regime as shown in Figure 4a. However, as shown in Figure 4b, there was a stronger correlation between ionic conductivity and glass transition temperature than between ionic conductivity and dielectric constant. Ionic conductivity at 60 °C was highest for the lowest- $T_{\rm g}$ polymer, PAGE, and decreased by an order of magnitude with a ca. 40 °C increase in T_g . This trend was similarly apparent when ionic conductivity at 60 °C (333 K) was plotted versus $T-T_{\rm g}$ (Figure 4c). The ionic conductivity increased with $T - T_o$; however, there was significant variability at lower values, which was likely due to the significant chemical diversity in the series of materials. The notion that low T_{σ} is required for high ionic conductivity is true only for high-dielectric-constant polymer hosts. For materials with lower dielectric constant, ion dissociation is limited by polarity, and ionic conductivity increases with dielectric constant. The T_g should be far below the use temperature to maintain rapid segmental dynamics; however, $T_{\rm g}$ is otherwise not a governing parameter. To complicate interpretation, a correlation also exists between dielectric constant and T_g , with higher dielectric constants leading generally to a higher T_g values (Figure 4d). This result can be rationalized based on the predictive simulations of Wheatle et al. which showed that, regardless of the specific chemical makeup of the polymer, increasing dielectric constant led to stronger polymer-polymer and polymer-ion interactions. These stronger interactions would be expected to increase T_g with or without ions, which we observe here in our homologous series of high-polarity, low- T_g polyethers.

To put these results into a broader context, the previous report by Imbrogno et al. 47 experimentally validated the coarse-grained simulations by Wheatle et al. 7 in the low-dielectric-constant regime by demonstrating increases in ionic conductivity with increasing dielectric constant. The current work provides additional experimental validation of the coarse-grained simulation predictions by extending further into the higher-dielectric-constant regime where conductivity is expected to decrease with increasing dielectric constant. The ionic conductivity reaches an optimum at a dielectric constant of ca. 9 for a polymer electrolyte host. At this point, ion

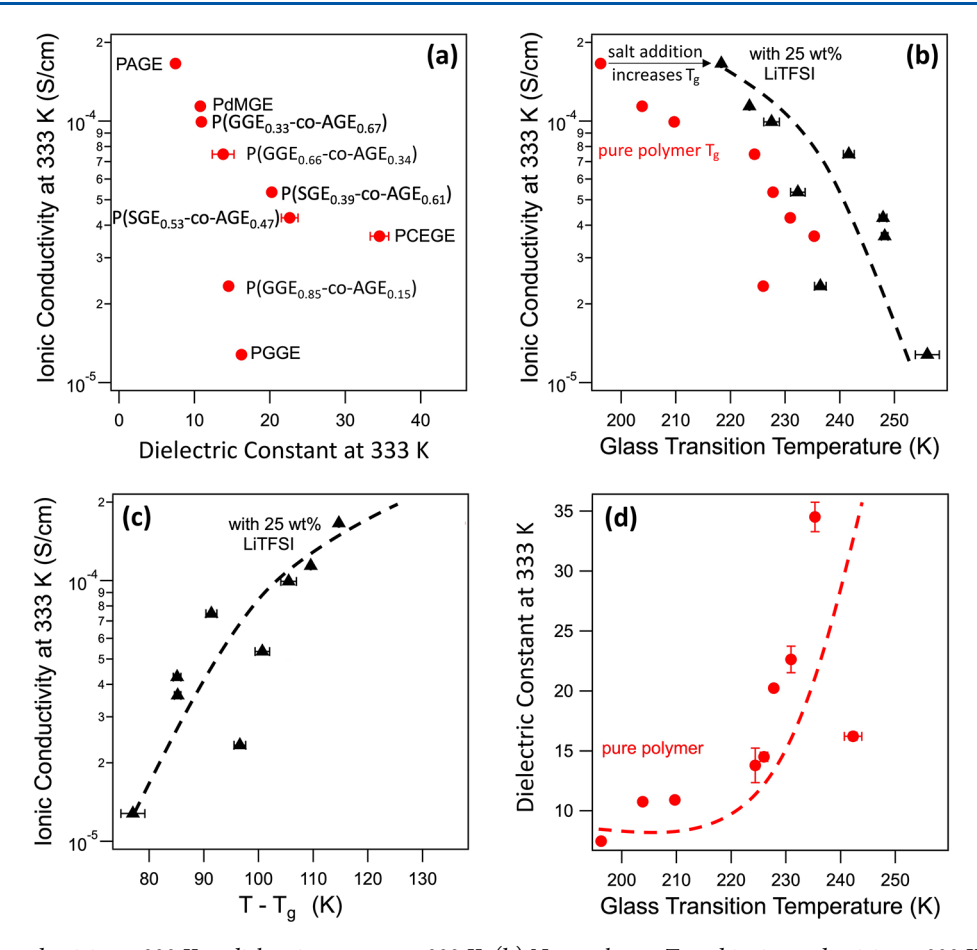


Figure 4. (a) Ionic conductivity at 333 K vs dielectric constant at 333 K. (b) Neat polymer $T_{\rm g}$ and ionic conductivity at 333 K vs polymer with 25 wt % LiTFSI $T_{\rm g}$. All glass transition temperatures increased with the addition of 25 wt % LiTFSI. (c) Ionic conductivity at 333 K vs $T - T_{\rm g}$ for polymers with 25 wt % LiTFSI. (d) Dielectric constant at 333 K vs $T_{\rm g}$ for polymers with 25 wt % LiTFSI. Dotted lines are drawn to guide the eye.

dissociation is balanced by rapid segmental dynamics. With further increases in dielectric constant, ionic conductivity decreases due to increasing polymer host $T_{\rm g}$. This decrease in conductivity was shown in simulation to arise from stronger intra- and interchain polymer interactions, slowing polymer segmental dynamics and restricting the movement of ions solvated in the polymer matrix. The coarse-grained simulations incorporated only the dipole moment of the monomers comprising the polymer chains without the specific chemical makeup of the repeat units. The validation of the coarsegrained simulation using experimental data from a variety of different polymers with different side chain functionality supports the generality of this physical insights reported here. Our results, when combined with the low-dielectricconstant regime results of Imbrogno et al.,⁴⁷ suggest that the results of Wheatle et al.7 are generalizable to single polyetherbased electrolyte systems with nonspecific interactions between the polymers and dissolved ions. With this conclusion in mind, future development of polymer electrolytes with neutral polymer hosts should focus on polymer blends or copolymers that can potentially provide both high polarity and rapid segmental dynamics or alternative strategies beyond single-component, neutral polymer hosts.

CONCLUSIONS

Predictive molecular dynamics simulations by Wheatle et al. presented two regimes of structure—property relationships governing ionic conductivity in single polymer electrolytes.⁷

The low-dielectric-constant regime was explored in previous experimental works by Imbrogno et al., which demonstrated increasing ionic conductivity in polymer electrolytes with increasing polymer dielectric constant.⁴⁷ In the high-dielectricconstant regime of this study, ionic conductivity decreased with increasing polymer dielectric constant. At the crossover between these regimes an optimum occurs in ionic conductivity at a dielectric constant near that of amorphous poly(ethylene oxide) as ion dissociation is balanced by rapid segmental dynamics. To experimentally probe the highdielectric-constant regime, we synthesized nine polyethers with dielectric constants ranging from 7 to 35 at 60 °C and observed the expected decrease in ionic conductivity from 10⁻³ to 10^{-7} S/cm accompanied by an increase in glass transition temperature as polymer-polymer and polymer-ion interactions become stronger. To improve the ionic conductivity of polymer electrolytes, single-component polymer hosts are unlikely to resolve the trade-off between the need for ion dissociation and rapid segmental dynamics required for rapid ion diffusion to give high ionic conductivity. Blends of polymer hosts that combine high-polarity and low-viscosity components may ameliorate the transport limitations that arise in highpolarity polymer hosts.

ASSOCIATED CONTENT

Supporting Information

The Supporting Information is available free of charge at https://pubs.acs.org/doi/10.1021/acs.macromol.2c00639.

Experimental details and molecular—thermal characterization data including ¹H NMR spectroscopy, differential scanning calorimetry, size exclusion chromatography, broadband dielectric spectroscopy, and electrochemical impedance spectroscopy (PDF)

AUTHOR INFORMATION

Corresponding Authors

Benny D. Freeman — McKetta Department of Chemical Engineering, The University of Texas at Austin, Austin, Texas 78712, United States; Orcid.org/0000-0003-2779-7788; Email: freeman@che.utexas.edu

Venkat Ganesan — McKetta Department of Chemical Engineering, The University of Texas at Austin, Austin, Texas 78712, United States; ◎ orcid.org/0000-0003-3899-5843; Email: venkat@che.utexas.edu

Nathaniel A. Lynd — McKetta Department of Chemical Engineering, The University of Texas at Austin, Austin, Texas 78712, United States; Texas Materials Institute, The University of Texas at Austin, Austin, Texas 78712, United States; Occid.org/0000-0003-3010-5068; Email: lynd@che.utexas.edu

Authors

- Benjamin J. Pedretti McKetta Department of Chemical Engineering, The University of Texas at Austin, Austin, Texas 78712, United States
- Natalie J. Czarnecki McKetta Department of Chemical Engineering, The University of Texas at Austin, Austin, Texas 78712, United States
- Congzhi Zhu McKetta Department of Chemical Engineering, The University of Texas at Austin, Austin, Texas 78712, United States; orcid.org/0000-0002-1302-7187
- Jennifer Imbrogno McKetta Department of Chemical Engineering, The University of Texas at Austin, Austin, Texas 78712, United States
- Frederick Rivers McKetta Department of Chemical Engineering, The University of Texas at Austin, Austin, Texas 78712, United States

Complete contact information is available at: https://pubs.acs.org/10.1021/acs.macromol.2c00639

Notes

The authors declare no competing financial interest.

ACKNOWLEDGMENTS

This work was supported in part by grants from the Robert A. Welch Foundation under Grants F-1599 and F-1904 (C.Z. and N.A.L., characterization and materials and supplies support); the National Science Foundation under Grants CBET-1706968 (B.J.P., V.G., and N.A.L.) and CHE-2004167 (J.I. and N.A.L.); and the Center for Materials for Water and Energy Systems (M-WET), an Energy Frontier Research Center funded by the U.S. Department of Energy, Office of Science, Basic Energy Sciences, under Award # DE-SC0019272 (B.J.P., F.W.R., B.D.F., V.G., and N.A.L., synthesis, stipend support, and characterization).

REFERENCES

(1) Goodenough, J. B.; Kim, Y. Challenges for Rechargeable Li Batteries. *Chem. Mater.* **2010**, 22 (3), 587–603.

- (2) Xu, W.; Wang, J.; Ding, F.; Chen, X.; Nasybulin, E.; Zhang, Y.; Zhang, J.-G. Lithium Metal Anodes for Rechargeable Batteries. *Energy Env. Sci.* **2014**, *7* (2), 513–537.
- (3) Hall, D. S.; Self, J.; Dahn, J. R. Dielectric Constants for Quantum Chemistry and Li-Ion Batteries: Solvent Blends of Ethylene Carbonate and Ethyl Methyl Carbonate. *J. Phys. Chem. C* **2015**, *119* (39), 22322–22330.
- (4) Ue, M.; Sasaki, Y.; Tanaka, Y.; Morita, M. In *Electrolytes for Lithium and Lithium-Ion Batteries*; Jow, T. R., Xu, K., Borodin, O., Ue, M., Eds.; Modern Aspects of Electrochemistry; Springer: New York; 2014, Vol. 58, pp 93–165.
- (5) Xu, K. Nonaqueous Liquid Electrolytes for Lithium-Based Rechargeable Batteries. *Chem. Rev.* **2004**, *104* (10), 4303–4418.
- (6) Wheatle, B. K.; Keith, J. R.; Mogurampelly, S.; Lynd, N. A.; Ganesan, V. Influence of Dielectric Constant on Ionic Transport in Polyether-Based Electrolytes. *ACS Macro Lett.* **2017**, *6* (12), 1362–1367.
- (7) Wheatle, B. K.; Lynd, N. A.; Ganesan, V. Effect of Polymer Polarity on Ion Transport: A Competition between Ion Aggregation and Polymer Segmental Dynamics. ACS Macro Lett. 2018, 7 (10), 1149–1154
- (8) Wheatle, B. K.; Fuentes, E. F.; Lynd, N. A.; Ganesan, V. Influence of Host Polarity on Correlating Salt Concentration, Molecular Weight, and Molar Conductivity in Polymer Electrolytes. *ACS Macro Lett.* **2019**, *8* (8), 888–892.
- (9) Wheatle, B. K.; Lynd, N. A.; Ganesan, V. Effect of Host Incompatibility and Polarity Contrast on Ion Transport in Ternary Polymer-Polymer-Salt Blend Electrolytes. *Macromolecules* **2020**, *53* (3), 875–884.
- (10) Fenton, D. E.; Parker, J. M.; Wright, P. V. Complexes of Alkali Metal Ions with Poly(Ethylene Oxide). *Polymer* **1973**, *14*, 589.
- (11) Wright, P. V. Electrical Conductivity in Ionic Complexes of Poly(Ethylene Oxide). *Br. Polym. J.* **1975**, *7* (5), 319–327.
- (12) Scrosati, B.; Vincent, C. A. Polymer Electrolytes: The Key to Lithium Polymer Batteries. MRS Bull. 2000, 25 (3), 28–30.
- (13) Xue, Z.; He, D.; Xie, X. Poly(Ethylene Oxide)-Based Electrolytes for Lithium-Ion Batteries. *J. Mater. Chem. A* **2015**, 3 (38), 19218–19253.
- (14) Barteau, K. P.; Wolffs, M.; Lynd, N. A.; Fredrickson, G. H.; Kramer, E. J.; Hawker, C. J. Allyl Glycidyl Ether-Based Polymer Electrolytes for Room Temperature Lithium Batteries. *Macromolecules* **2013**, *46* (22), 8988–8994.
- (15) Mindemark, J.; Lacey, M. J.; Bowden, T.; Brandell, D. Beyond PEO—Alternative Host Materials for Li + -Conducting Solid Polymer Electrolytes. *Prog. Polym. Sci.* **2018**, *81*, 114–143.
- (16) Teran, A. A.; Tang, M. H.; Mullin, S. A.; Balsara, N. P. Effect of Molecular Weight on Conductivity of Polymer Electrolytes. *Solid State Ion.* **2011**, 203 (1), 18–21.
- (17) Trapa, P. E.; Won, Y.-Y.; Mui, S. C.; Olivetti, E. A.; Huang, B.; Sadoway, D. R.; Mayes, A. M.; Dallek, S. Rubbery Graft Copolymer Electrolytes for Solid-State, Thin-Film Lithium Batteries. *J. Electrochem. Soc.* 2005, 152 (1), A1.
- (18) Trapa, P. E.; Reyes, A. B.; Das Gupta, R. S.; Mayes, A. M.; Sadoway, D. R. Polarization in Cells Containing Single-Ion Graft Copolymer Electrolytes. *J. Electrochem. Soc.* **2006**, *153* (6), A1098.
- (19) Singh, M.; Odusanya, O.; Wilmes, G. M.; Eitouni, H. B.; Gomez, E. D.; Patel, A. J.; Chen, V. L.; Park, M. J.; Fragouli, P.; Iatrou, H.; Hadjichristidis, N.; Cookson, D.; Balsara, N. P. Effect of Molecular Weight on the Mechanical and Electrical Properties of Block Copolymer Electrolytes. *Macromolecules* **2007**, 40 (13), 4578–4585.
- (20) Panday, A.; Mullin, S.; Gomez, E. D.; Wanakule, N.; Chen, V. L.; Hexemer, A.; Pople, J.; Balsara, N. P. Effect of Molecular Weight and Salt Concentration on Conductivity of Block Copolymer Electrolytes. *Macromolecules* **2009**, 42 (13), 4632–4637.
- (21) Wong, D. T.; Mullin, S. A.; Battaglia, V. S.; Balsara, N. P. Relationship between Morphology and Conductivity of Block-Copolymer Based Battery Separators. *J. Membr. Sci.* **2012**, 394–395, 175–183.

- (22) Young, W.-S.; Kuan, W.-F.; Epps, T. H. Block Copolymer Electrolytes for Rechargeable Lithium Batteries. *J. Polym. Sci., Part B: Polym. Phys.* **2014**, *52* (1), 1–16.
- (23) Gao, K. W.; Loo, W. S.; Snyder, R. L.; Abel, B. A.; Choo, Y.; Lee, A.; Teixeira, S. C. M.; Garetz, B. A.; Coates, G. W.; Balsara, N. P. Miscible Polyether/Poly(Ether-Acetal) Electrolyte Blends. *Macromolecules* **2020**, *53* (14), 5728–5739.
- (24) Fish, D.; Khan, I. M.; Wu, E.; Smid, J. Polymer Electrolyte Complexes of LiCIO4 and Comb Polymers of Siloxane with Oligo-Oxyethylene Side Chains. *Br. Polym. J.* **1988**, *20* (3), 281–288.
- (25) Watanabe, M. Polymer Electrolytes Derived from Dendritic Polyether Macromonomers. *Solid State Ion.* **2002**, *148* (3–4), 399–404
- (26) Hawker, C. J.; Chu, F.; Pomery, P. J.; Hill, D. J. T. Hyperbranched Poly(Ethylene Glycol)s: A New Class of Ion-Conducting Materials. *Macromolecules* **1996**, 29 (11), 3831–3838.
- (27) Nishimoto, A.; Watanabe, M.; Ikeda, Y.; Kohjiya, S. High Ionic Conductivity of New Polymer Electrolytes Based on High Molecular Weight Polyether Comb Polymers. *Electrochim. Acta* **1998**, 43 (10–11), 1177–1184.
- (28) Sun, J.; Stone, G. M.; Balsara, N. P.; Zuckermann, R. N. Structure-Conductivity Relationship for Peptoid-Based PEO-Mimetic Polymer Electrolytes. *Macromolecules* **2012**, *45* (12), 5151–5156.
- (29) Snyder, R. L.; Choo, Y.; Gao, K. W.; Halat, D. M.; Abel, B. A.; Sundararaman, S.; Prendergast, D.; Reimer, J. A.; Balsara, N. P.; Coates, G. W. Improved Li ⁺ Transport in Polyacetal Electrolytes: Conductivity and Current Fraction in a Series of Polymers. *ACS Energy Lett.* **2021**, *6* (5), 1886–1891.
- (30) Halat, D. M.; Snyder, R. L.; Sundararaman, S.; Choo, Y.; Gao, K. W.; Hoffman, Z. J.; Abel, B. A.; Grundy, L. S.; Galluzzo, M. D.; Gordon, M. P.; Celik, H.; Urban, J. J.; Prendergast, D.; Coates, G. W.; Balsara, N. P.; Reimer, J. A. Modifying Li ⁺ and Anion Diffusivities in Polyacetal Electrolytes: A Pulsed-Field-Gradient NMR Study of Ion Self-Diffusion. *Chem. Mater.* **2021**, 33 (13), 4915–4926.
- (31) Long, L.; Wang, S.; Xiao, M.; Meng, Y. Polymer Electrolytes for Lithium Polymer Batteries. *J. Mater. Chem. A* **2016**, 4 (26), 10038–10069.
- (32) Armand, M. The History of Polymer Electrolytes. Solid State Ion. 1994, 69 (3-4), 309-319.
- (33) Chen, G.; Bai, Y.; Gao, Y.; Wang, Z.; Zhang, K.; Ni, Q.; Wu, F.; Xu, H.; Wu, C. Inhibition of Crystallization of Poly(Ethylene Oxide) by Ionic Liquid: Insight into Plasticizing Mechanism and Application for Solid-State Sodium Ion Batteries. *ACS Appl. Mater. Interfaces* **2019**, *11* (46), 43252–43260.
- (34) Kumar, Y.; Hashmi, S. A.; Pandey, G. P. Lithium Ion Transport and Ion-Polymer Interaction in PEO Based Polymer Electrolyte Plasticized with Ionic Liquid. *Solid State Ion.* **2011**, *201* (1), 73–80.
- (35) Widstrom, M. D.; Ludwig, K. B.; Matthews, J. E.; Jarry, A.; Erdi, M.; Cresce, A. V.; Rubloff, G.; Kofinas, P. Enabling High Performance All-Solid-State Lithium Metal Batteries Using Solid Polymer Electrolytes Plasticized with Ionic Liquid. *Electrochim. Acta* **2020**, *345*, 136156.
- (36) Jones, S. D.; Nguyen, H.; Richardson, P. M.; Chen, Y.-Q.; Wyckoff, K. E.; Hawker, C. J.; Clément, R. J.; Fredrickson, G. H.; Segalman, R. A. Design of Polymeric Zwitterionic Solid Electrolytes with Superionic Lithium Transport. ACS Cent. Sci. 2022, 8, 169.
- (37) Brown, J. R.; Seo, Y.; Hall, L. M. Ion Correlation Effects in Salt-Doped Block Copolymers. *Phys. Rev. Lett.* **2018**, *120* (12), 127801.
- (38) Seo, Y.; Shen, K.-H.; Brown, J. R.; Hall, L. M. Role of Solvation on Diffusion of Ions in Diblock Copolymers: Understanding the Molecular Weight Effect through Modeling. *J. Am. Chem. Soc.* **2019**, 141 (46), 18455–18466.
- (39) Shen, K.-H.; Hall, L. M. Ion Conductivity and Correlations in Model Salt-Doped Polymers: Effects of Interaction Strength and Concentration. *Macromolecules* **2020**, *53* (10), 3655–3668.
- (40) Frech, R.; York, S.; Allcock, H.; Kellam, C. Ionic Transport in Polymer Electrolytes: The Essential Role of Associated Ionic Species. *Macromolecules* **2004**, *37* (23), 8699–8702.

- (41) Gudla, H.; Shao, Y.; Phunnarungsi, S.; Brandell, D.; Zhang, C. Importance of the Ion-Pair Lifetime in Polymer Electrolytes. *J. Phys. Chem. Lett.* **2021**, *12* (35), 8460–8464.
- (42) Mullin, S. A.; Stone, G. M.; Panday, A.; Balsara, N. P. Salt Diffusion Coefficients in Block Copolymer Electrolytes. *J. Electrochem. Soc.* **2011**, *158* (6), A619.
- (43) Chintapalli, M.; Timachova, K.; Olson, K. R.; Mecham, S. J.; Devaux, D.; DeSimone, J. M.; Balsara, N. P. Relationship between Conductivity, Ion Diffusion, and Transference Number in Perfluor-opolyether Electrolytes. *Macromolecules* **2016**, 49 (9), 3508–3515.
- (44) Choo, Y.; Halat, D. M.; Villaluenga, I.; Timachova, K.; Balsara, N. P. Diffusion and Migration in Polymer Electrolytes. *Prog. Polym. Sci.* **2020**, *103*, 101220.
- (45) Mongcopa, K. I. S.; Tyagi, M.; Mailoa, J. P.; Samsonidze, G.; Kozinsky, B.; Mullin, S. A.; Gribble, D. A.; Watanabe, H.; Balsara, N. P. Relationship between Segmental Dynamics Measured by Quasi-Elastic Neutron Scattering and Conductivity in Polymer Electrolytes. *ACS Macro Lett.* **2018**, 7 (4), 504–508.
- (46) Hoffman, Z. J.; Shah, D. B.; Balsara, N. P. Temperature and Concentration Dependence of the Ionic Transport Properties of Poly(Ethylene Oxide) Electrolytes. *Solid State Ion.* **2021**, *370*, 115751.
- (47) Imbrogno, J.; Maruyama, K.; Rivers, F.; Baltzegar, J. R.; Zhang, Z.; Meyer, P. W.; Ganesan, V.; Aoshima, S.; Lynd, N. A. Relationship between Ionic Conductivity, Glass Transition Temperature, and Dielectric Constant in Poly(Vinyl Ether) Lithium Electrolytes. *ACS Macro Lett.* **2021**, *10* (8), 1002–1007.
- (48) Luu, H.-T.; Wiesler, S.; Frey, G.; Streuff, J. A Titanium(III)-Catalyzed Reductive Umpolung Reaction for the Synthesis of 1,1-Disubstituted Tetrahydroisoquinolines. *Org. Lett.* **2015**, *17* (10), 2478–2481.
- (49) Rodriguez, C. G.; Ferrier, R. C.; Helenic, A.; Lynd, N. A. Ring-Opening Polymerization of Epoxides: Facile Pathway to Functional Polyethers via a Versatile Organoaluminum Initiator. *Macromolecules* **2017**, *50* (8), 3121–3130.
- (50) Ferrier, R. C.; Imbrogno, J.; Rodriguez, C. G.; Chwatko, M.; Meyer, P. W.; Lynd, N. A. Four-Fold Increase in Epoxide Polymerization Rate with Change of Alkyl-Substitution on Mono-μ-Oxo-Dialuminum Initiators. *Polym. Chem.* **2017**, 8 (31), 4503–4511.
- (51) Miller, K. A.; Morado, E. G.; Samanta, S. R.; Walker, B. A.; Nelson, A. Z.; Sen, S.; Tran, D. T.; Whitaker, D. J.; Ewoldt, R. H.; Braun, P. V.; Zimmerman, S. C. Acid-Triggered, Acid-Generating, and Self-Amplifying Degradable Polymers. *J. Am. Chem. Soc.* **2019**, *141* (7), 2838–2842.
- (52) Berridge, M. S.; Franceschini, M. P.; Rosenfeld, E.; Tewson, T. J. Cyclic Sulfates: Useful Substrates for Selective Nucleophilic Substitution. *J. Org. Chem.* **1990**, *55* (4), 1211–1217.
- (53) Zhang, C.; Hutter, J.; Sprik, M. Computing the Kirkwood *g*-Factor by Combining Constant Maxwell Electric Field and Electric Displacement Simulations: Application to the Dielectric Constant of Liquid Water. *J. Phys. Chem. Lett.* **2016**, *7* (14), 2696–2701.
- (\$4) Kirkwood, J. G. The Dielectric Polarization of Polar Liquids. J. Chem. Phys. 1939, 7 (10), 911–919.
- (55) Onsager, L. Electric Moments of Molecules in Liquids 1936, 58, 8.